We are IntechOpen, the world's leading publisher of Open Access books Built by scientists, for scientists

4,800
Open access books available

122,000
International authors and editors

135M
Downloads

Our authors are among the

154
Countries delivered to

TOP 1%
most cited scientists

12.2%
Contributors from top 500 universities

CLARIVATE ANALYTICS BOOK CITATION INDEX INDEXED

WEB OF SCIENCE™

Selection of our books indexed in the Book Citation Index in Web of Science™ Core Collection (BKCI)

Interested in publishing with us?
Contact book.department@intechopen.com

Numbers displayed above are based on latest data collected.
For more information visit www.intechopen.com

16

Cholesteric Elastomers with Mechanical Control of Optical Spectra

J. Adrián Reyes[1], Laura O. Palomares[2] and Carlos G. Avendaño[3]
[1]*Universidad Autónoma Metropolitana (on leave from Instituto de Fisica, UNAM) Ixtapalapa, Apartado,*
[2]*Research Institute for Solid State Physics and Optics of the Hungarian Academy of Sciences, H-1525 Budapest,*
[3]*Universidad Autónoma de la Ciudad de México,*
[1,3]*México*
[2]*Hungary*

1. Introduction

Elastomers are elastic media which mixes as no one, also, they have three important properties: orientational order of large range in amorphous soft materials, macroscopic susceptibility to the molecular shape, and quenching to the topological constraints. Classical liquid crystals are fluids typically composed by rigid molecules, which with a continuous model, are represented by bars and exhibit an orientational order of large range. The simplest order displayed by these systems is the nematic, for which, all the molecules are aligned in average. Complementary, the polymeric long chains embodying anisotropic rigid units can be nematically aligned and may form polymeric liquid crystals.

However, the long chains are elongated when their rigid monomeric components are oriented, giving rise to an anisotropic material. If additionally, the polymeric chains are joint to a backbone in such way that their topology is restrained, hence the melt condenses in a very elastic solid or rubber. It is convenient to mention that in general, within the rubbers, the nematic monomeric molecules retain the same mobility as in a liquid phase.

These soft constrictions make the resulting material, which is then a solid very extensible. Rubbers resist mechanic deformations since the polymeric chains reach their maximum entropy when they stay in their natural state without deformation. The polymerization of these compounds creates links between the chains which joint to the backbone formed collectively among themselves.

It is to be expected that in this process, the anisotropic rigid units of nematic character, for instance (nematogens) which lie in the inner of the medium, form spontaneously domains distributed in all the rubber, whose preferred orientation is to be in different directions. This variety of domains causes light scattering giving rise to a macroscopic turbid appearance to the material. One very important advance in the design of these materials was managed by Finkelman, by developing a procedure for obtaining samples which form a single domain. The basic idea consists in applied electric field to the melt substance in order to align the anisotropic monomeric units while the polimerization is taking place and/or the temperature

is decreased to maintain the orientational order of the oriented nematic elements and in turn attain a monodomain.

A material prepared in this way is called as a liquid crystal elastomer and has the amazing property of being deformable, within certain interval of elongations, investing in this a practically negligible amount of energy. This is caused essentially by the reorientation and accommodation of the anisotropic structure formed by the rigid nematic monomers or other mesophases in the inner of long polymeric chains while the material is distorted in such way that the energy utilized is minimized when the mentioned structure turns.

Nowadays the liquid crystal elastomers are synthesized to generate phases of the same variety obtained with classical liquid crystals. It can be created nematics, smectic and chiral liquid crystals. Similarly to any polymeric rubber, the materials are very deformable since their dimensions can be changed under the influence of external stresses as much as 300% of their original sizes. They can be easily oriented by electrical fields as the ordinary liquid crystals. Both features make of these new materials excellent candidates to design artificial muscles. On the other hand, their transparency in the monodomain phase and the fact that as solids do not require a container make them excellent candidates to be used as electro optic devices.

2. Polymers

2.1 Polymer configuration

A polymer is a very long chain formed by many repeated molecular units, as much as thousands, called monomers. All polymeric chains possess a characteristic length l, at which the chains can be bended. This length can contain various monomers when the total number of monomers in the chain N is much larger than the number of monomers per length l and then we can affirm that there exist various possible spatial configurations for the polymer. Thus, it is possible to employ a Gaussian distribution to describe adequately the system. Here we shall assume that this is the case.

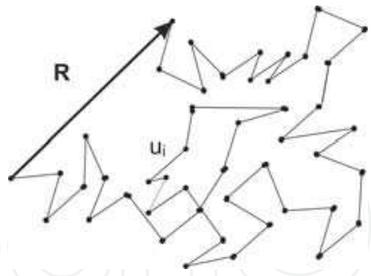

Fig. 1. A chain composed by N bar of length a freely joint is statistically equivalent to the path of a random walk with fixed step a.

A chain composed by N bar of length a freely joint like the one shown in Fig. 1 is statistically equivalent to the path of a random walk with fixed step a. The average mean square of the end to end vector $\mathbf{u}_l$ formed after this walk of N steps (Warner & Terentjev, 2003)

$$\langle \mathbf{R}_x^2 \rangle = \langle \mathbf{R}_y^2 \rangle = \langle \mathbf{R}_z^2 \rangle = \frac{1}{3}\langle \mathbf{R}^2 \rangle = \frac{1}{3}a^2 N \equiv \frac{1}{3}aL, \tag{1.1}$$

where $L = Na$ is the total length of the chain. In terms of the end to end vector which joint the monomers $\mathbf{u}_i$ of length a, the distance between the two edges of the chain is given by the

magnitude of the vector: $\mathbf{R} = \Sigma_i \mathbf{u}_i$. This quantity is very important since provides a notion of the spatial configuration of the polymer chains and from the polymer chain distribution we can derive the free energy characterizing the system. The vectors $\mathbf{u}_i$ are not correlated each other so that $\langle \mathbf{u}_i \mathbf{u}_j \rangle = \delta_{ij} a^2$ which is consistent with Eq. (1.1).

A polymer is a thermodynamical system in equilibrium interacting with its surrounding at volume and temperature constants. Hence, the total number of possible conformations of one given chain Z_N (or the number of possible random walk without restrictions) must be equal to the partition function of the chain: $Z_N = \Sigma_{config} e^{-H/kT}$, where H is the energy of the configuration, k is the Boltzmann constant and T is the temperature. If we take a random walk for which the two ends of the walks are fixed, we expect that the number of possible configurations is to be smaller than that of the system just mentioned. Thus the number of configurations for fixed boundary conditions is given by

$$Z_N(\mathbf{R}) = p_N(\mathbf{R}) Z_N \,, \tag{1.2}$$

where $p_N(\mathbf{R})$ is the probability of having a configuration with an end to end vector $\mathbf{R}$. Since Z_N is the partition function of the system, the probability of distribution must be Gaussian and as a consequence its explicit normalized expression is given by (Kac et al., 1976):

$$p_N(\mathbf{R}) = \left(\frac{3}{2\pi R_o^2} \right)^{3/2} e^{-3\mathbf{R}^2 / 2R_o^2} \,, \tag{1.3}$$

Where R_o is the variance of the system and from Eq. (1.1) we get $R_o^2 = aL$.

The fact that the polymer chain is kept at volume and temperature constants allow us to use the Helmholtz free energy to describe the system which in agreement with the statistical physics is given by $F = -k_B T ln Z_N(\mathbf{R})$; substitution of Eqs. (1.2) and (1.3) in this expression, yields

$$F(\mathbf{R}) = F_o + k_B T \left(\frac{3\mathbf{R}^2}{2R_o^2} \right) + C \,, \tag{1.4}$$

where $F_o = -k_B T ln Z_N$ is the free energy of the polymeric chain without restrictions in their ends and C is the constant coming from the normalization of the distribution P_N,.F_o and C are constants independent of $\mathbf{R}$, which only determine the reference point, thus their values are irrelevant to find the minimum of the free energy of the system. We remark that the energy given in Eq. (1.4) is purely entropic since only depends on the number of possible configuration of the systems. To obtain this expression we assume that all the possible configurations contribute with the same energy and we neglect the chemical energy caused by the electromagnetic repulsion between the molecules. If we take into account the internal energy associated with chemical processes, $U(\mathbf{R})$, the free energy of the system is given by

$$F(\mathbf{R}) = U(\mathbf{R}) - TS(\mathbf{R}) \,, \tag{1.5}$$

where the entropy per molecule is represented $S(\mathbf{R})$. Strictly speaking, this term should be considered however it has been shown that the entropy (Warner & Terentjev, 2003) dominates the free energy and then we can neglect it, $S(R) = -3k_B \mathbf{R}^2 / 2R_o^2$.

2.2 Polymeric liquid crystals

A polymeric liquid crystal combines the spontaneous orientation of the liquid crystals with the elasticity governed by entropy discussed above. It is necessary a delicate balance in these properties to create a polymeric liquid crystal.

2.2.1 Polymeric liquid crystals shape

The average shape of the polymeric main chain is crucial since this is responsible of the equilibrium elastic response of the network it belongs. Some ordinary polymers are isotropic or spheric so that only one dimension is enough to characterize these materials. In contrast, the nematic polymers may adopt diverse shapes due to the fact that the average backbone is distorted by the reorientation suffered by the molecular bars guided by the director $\mathbf{n}$, that is, the nematic order modifies the backbone form of the polymer. Hence, nematic polymers require more than one direction to describe their anisotropic form.

To characterize the chain form and its probability distribution the quadratic mean square of shape is given by

$$\langle R_i R_j \rangle = \frac{1}{3} l_{ij} L, \tag{1.6}$$

where we have defined l_{ij} as the effective length steps in distinct directions. For uniaxial polymers $\langle R_i R_j \rangle$, is the same for every perpendicular direction to $\mathbf{n}$. Thus, if $\mathbf{n}$ is along the z-axis, where $R_x = R_y = R_\perp$ and the tensor $\boldsymbol{l}$ for this case is

$$\mathbf{l}_o = \begin{pmatrix} l_\perp & 0 & 0 \\ 0 & l_\perp & 0 \\ 0 & 0 & l_\parallel \end{pmatrix}, \tag{1.7}$$

where $l_\perp$ and $l_\parallel$ are the length steps in the directions parallel and perpendicular to $\mathbf{n}$, respectively. In general, when $\mathbf{n}$ is not necessarily aligned with one of the axes of our reference system, the matrix $\mathbf{l}$ is not necessarily diagonal but uniaxial and has the form:

$$\mathbf{l}_o = l_\perp(\boldsymbol{\delta} + [r-1]\mathbf{nn}) \quad \text{and} \quad \mathbf{l}_o^{-1} = l_\perp(\boldsymbol{\delta} + [\frac{1}{r} - 1]\mathbf{nn}), \tag{1.8}$$

where we have defined the radius r, as the ratio between parallel and perpendicular effective length steps as $r = l_\parallel / l_\perp$.

If $r > 1$, means that we have a prolate backbone, which is larger along the direction $\mathbf{n}$; Instead for $r < 1$, we have an oblate, whose backbone is larger in perpendicular plane to $\mathbf{n}$.

The probability of find a configuration with end to end vector: $\mathbf{R}$, Eq. (1.3). On the other hand the probability of find certain configuration for the anisotropic case, is obtained by using Eq. (1.1) from which it can be derived $R_o^2 = l_{ij} L$ and $\mathbf{R}^2 = R_i R_j$. By substituting these expressions in Eq. (1.3), we get the probability for the anisotropic case:

$$p(\mathbf{R}) = \left[\left(\frac{3}{2\pi L} \right)^3 \frac{1}{Det[\mathbf{l}]} \right]^{1/2} e^{\left(\frac{-3}{2L} R_i l_{ij}^{-1} R_j \right)}. \tag{1.9}$$

3. Nematic rubber elasticity

Nematic elastomer systems can be quite elastic, that is they can be extended or compressed for large proportions. The difference between nematic and isotropic rubbers is the molecular shape anisotropy induced by liquid crystal order. The simplest description of nematic rubbers is arising from extension of the molecular theory of rubbers just discussed in the foregoing section and is known as the neoclassic theory.

The number of configurations in one thread connecting two crosslinkings separated by a distance $\mathbf{R}$ in one nematic rubber is proportional to the anisotropic Gaussian distribution given by Eq. (1.9).

The step length vector $\mathbf{l}$ reflexes the actual nematic order in the rubber. In contrast, in the formation state the end to end vector is $\mathbf{R}_f$ and the shape of the chains in that state is similarly described by Gaussian distribution whose form is the same as Eq. (1.9) but with step length vector $\mathbf{l}_o$. One reason for having a different distribution is that the temperature changes and thus the nematic order as well. If the starting state is nematic, then an orientation change can also modified the distribution. As before, let us consider that a total deformation $\boldsymbol{\eta}_t$ affine leads from the formation state $\mathbf{R}_f$ to the actual situation $\mathbf{R} = \boldsymbol{\eta}_t \cdot \mathbf{R}$. The free energy, is obtained by averaging over a ensemble of initial condition whose energy of formation are the same

$$\mathcal{F} = -k_B T \left\langle \ln p(\mathbf{R}) \right\rangle_{p_0(\mathbf{R}_f)} = \frac{3k_B T}{2L} \left\langle \mathbf{R} \cdot \mathbf{l}^{-1} \cdot \mathbf{R} \right\rangle + \frac{k_B T}{2} \ln\left(\frac{Det[\mathbf{l}]}{a^3} \right), \tag{1.10}$$

the term in $Det[\mathbf{l}]$ is due to the normalization factor containing the information of the nematic order by means of the step length tensor $\mathbf{l}$. The free energy can be rewritten as

$$\mathcal{F} = \frac{3k_B T}{2L} \left\langle \mathbf{R}_f \cdot \boldsymbol{\eta}^T \cdot \mathbf{l}^{-1} \cdot \boldsymbol{\eta} \cdot \mathbf{R}_f \right\rangle_{p_0} \tag{1.11}$$

The average over the set of formation states can be performed directly using the relation $\left\langle \mathbf{R}_f \mathbf{R}_f \right\rangle_{p_0(\mathbf{R}_f)} = \mathbf{l}_o L / 3$, so that the average energy per thread is finally

$$\mathcal{F} = \frac{k_B T}{2} Tr\left(\mathbf{l}_o \cdot \boldsymbol{\eta}^T \cdot \mathbf{l}^{-1} \cdot \boldsymbol{\eta} \right) + \frac{k_B T}{2} \ln\left(\frac{Det[\mathbf{l}]}{a^3} \right). \tag{1.12}$$

This expression is a generalization of the classical free energy for the elasticity for a thread for which is known as the neoclassic free energy. To obtain the whole free energy of the rubber we need to count the number of threads per volume n_s, that is $F = n_s \mathcal{F}$ and since the linear shear modulus of a rubber is $\mu = n_s k_B T$. The free energy density is given by

$$F = \frac{\mu}{2} Tr\left(\mathbf{l}_o \cdot \boldsymbol{\eta}^T \cdot \mathbf{l}^{-1} \cdot \boldsymbol{\eta} \right) \tag{1.13}$$

This expression is valid for all the deformation, including the larger ones, but it cannot describe those deformations which can stretch totally the polymeric chains. This expression involves the orientational information about the initial state $\mathbf{n}_0$ and actual state $\mathbf{n}$ of the

elastomer by means of $\mathbf{l}_o$ and $\mathbf{l}$. By contrary the free energy of ordinary nematic liquid crystal only depends on the actual state of distortion. Eq. (1.13) exhibits a complex structure since the distortions appear expressed in terms of the combination $\boldsymbol{\eta}^T \cdot \mathbf{l}^{-1} \cdot \boldsymbol{\eta}$.

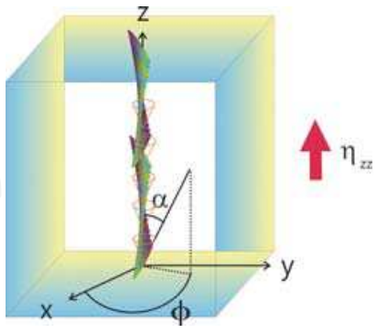

Fig. 2. A cholesteric elastomer submitted to distortion along its chiral axis, which in this case we chose to be the $z-$ axis.

4. Chiral elastomer under an axial deformation

Let us consider a cholesteric elastomer submitted to distortion along its chiral axis, which in this case we chose to be the z-axis, as shown in Fig. 2.
The deformation tensor, in its simplest, can be expressed as (Warner & Terentjev, 2003):

$$\boldsymbol{\eta} = \begin{pmatrix} 1/\sqrt{\eta} & 0 & \eta_{xz} \\ 0 & 1/\sqrt{\eta} & \eta_{yz} \\ 0 & 0 & \eta \end{pmatrix}, \tag{1.14}$$

where we have simplified the notation by the convention $\eta_{zz} = \eta$, as we discussed above, to keep the volume fixed , it is necessary to ask for $Det\boldsymbol{\eta} = 1$, which is straightforwardly fulfil by this expression since $Det\boldsymbol{\eta} = \frac{1}{\sqrt{\eta}}\frac{1}{\sqrt{\eta}}\eta = 1$. The terms η_{xz} and η_{yz}, are coming from the fact that we allow the director to rotate in the plane *x*-*y* which will be modified by expanding the elastomer along the *z*-axis.
The initial elastomer vector without deformation is given by: $\mathbf{n}_o = \{\cos q_o z, \sin q_o z, 0\}$, where $q_o = 2\pi / p$ is the helix wave number and p is the spatial periodicity or pitch. After the deformation, the director will be rotated by the angle $\omega = \frac{\pi}{2} - \alpha$, in such way that it lies over the surface of a cone Fig. 2; the new vector after deformation can be expressed as $\mathbf{n} = \{\sin\alpha\cos qz, \sin\alpha\sin qz, \cos\alpha\}$, where $q = q_0 / \eta$ is the new helix wave number scaled by the strain η; the initial step length vector without deformation, $\mathbf{l}_o$, is defined in agreement with Eq. (1.8) in terms of $\mathbf{n}_o$ and the inverse tensor is similar to Eq. (1.8) by replacing the vectors $\mathbf{n}$ by $\mathbf{n}_o$.

The Helmholtz free energy of the system is given by Eq. (1.13) in terms of $\mathbf{l}_o$ and $\mathbf{l}^{-1}$ of Eq. (1.8). Upon expansion of the Helmholtz free energy we can express this as

$$F = \mathbf{x}^T \cdot \mathbf{A} \cdot \mathbf{x} + \mathbf{b} \cdot \mathbf{x} + c \tag{1.15}$$

where

$$\mathbf{A} = \begin{pmatrix} \frac{1+3r+(r-1)\cos 2\alpha - 2(r-1)\cos 2qz\sin^2\alpha}{4r} & -\frac{(r-1)\sin 2qz\sin^2\alpha}{2r} \\ -\frac{(r-1)\sin 2qz\sin^2\alpha}{2r} & \frac{1+3r+(r-1)\cos 2\alpha + 2(r-1)\cos 2qz\sin^2\alpha}{4r} \end{pmatrix},$$

$$\mathbf{b} = \{-\frac{(r-1)\eta\cos qz\sin 2\alpha}{r}, \frac{(r-1)\eta\sin qz\sin 2\alpha}{r}\},$$

$$c = \frac{\eta^3 + r(3+r+\eta^3) + (r-1)(r-\eta^3)\cos 2\alpha}{2r\eta}$$

and $\mathbf{x} = \{\eta_{xz}, \eta_{yz}\}$. Eq. (1.15) represents the free energy of our system; it contains the information of the deformation. To find the state of deformation after a relaxation it is necessary to find the minimum of the free energy. When we extend an elastomer, first the strains are relaxed and after that the molecules will reorient. The minimum of energy is found by searching the values η_{xz} and η_{yz} which minimize the energy and then the optimum value of α.

To this purpose, we find the minimum with respect to η_{xz} and η_{yz} by diagonalizing the matrix A and translating to the principal axes system of the deformation (where we have denoted the strains by: η'_{xz} and η'_{yz}). Using the fact the minimum of system's energy is the same in any frame. Once doing this we find

$$\frac{2}{\mu}F = \eta^2 + \frac{1}{\eta} + \eta_{yz}^{\prime 2} - \frac{1}{2r}([r+1+(r-1)\cos 2\alpha](\eta^2 - \frac{r}{\eta} - \eta_{xz}^{\prime 2}) + 2(r-1)\eta\eta'_{xz}\sin 2\alpha - 2\eta^2, \tag{1.16}$$

This free energy depends on the strains and the angle. These variables used to be coupled to keep constant the free energy and cause a soft elasticity for which the elastomer is to be deformed at no energy cost. For this reason we minimize the energy by using two steps. We first find the minimum of Eq. (1.16) with respect to the strains and then minimize the resulting expression with respect to the angle. Performing the first step, we get from (1.16):

$$\eta'_{yz} = 0 \quad \text{and} \quad \eta'_{xz} = \eta\frac{(r-1)\sin 2\alpha}{(r+1)+(r-1)\cos 2\alpha}. \tag{1.17}$$

Notice that this expression allows to write the strains in terms of the orientation angle. Thus, after substitution of this expression in Eq. (1.16) we obtain the following expression which only depends on the angle α:

$$F = \frac{1}{2}\mu\left(\frac{2\eta^2}{r+1+(r-1)\cos 2\alpha} + \frac{3+r+1+(r-1)\cos 2\alpha}{2\eta}\right). \tag{1.18}$$

It remains to know the value of α that minimizes the latter expression. The director vector **n** will incline towards the *z*-direction with an angle ω (see Fig. 2) after the deformation, to find the value of ω, we minimize the free energy Eq. (1.18) we respect to ω, we get:

$$\cos 2\omega = \frac{r+1-2\eta^{3/2}}{r-1}; \qquad \omega(\eta) = \arcsin\sqrt{\frac{\eta^{3/2}-1}{r-1}}\,. \tag{1.19}$$

The latter equation indicates which is the degree of reorientation of the cholesteric, the maximum deformation is reached when the director vector aligns totally parallel to the *z*-axis, that is, when $\omega = \pi/2$, we find that $\eta = r^{2/3}$; when there is no deformation $\eta = 1$ and $\omega = 0$.

5. Propagation of waves in a layered medium

Optical propagation in layered media can be studied by conveniently writing Maxwell's equations in a 4×4 matrix. First, we show that in this matrix representation the boundary conditions of waves impinging on material can be imposed in a simpler way in such a way the transfer and scattering matrix formalism can be used in a natural way to obtain the transmittances and reflectances (Chuang, 2009; Hecht & Zajac, 1986). Next, we analytically solve the problem of axial propagation of an electromagnetic wave through a cholesteric elastomer by solidly rotating the laboratory reference system along the axial direction in the same way as the director **n**. Finally, we compute the optical spectra of a cholesteric elastomer under the influence of an externally induced mechanical strain.

5.1 4 x 4 Matrix representation

The transversality of electromagnetic waves suggest to rewrite the well known Maxwell equations in a representation which permits to analyze, at the same time, the behaviour of the four transversal components (2 components for electric field $\bar{E}$ and 2 components for magnetic field $\bar{H}$). This formalism is frequently referred to as Marcuvitz-Schwinger representation (Marcuvitz & Schwinger, 1951). If we define the four-vector

$$\boldsymbol{\Psi}(x,y,z) = \boldsymbol{\beta}(z)e^{i(k_x x+k_y y)-i\omega t} = \begin{pmatrix} e_x \\ e_y \\ h_x \\ h_y \end{pmatrix} e^{i(k_x x+k_y y)} e^{-i\omega t}, \tag{1.20}$$

with ω the angular frequency of the propagating wave and k_x, k_y the transversal components of wavevector. Maxwell's equations, inside a non-magnetic medium, can be written as:

$$\frac{\partial \boldsymbol{\beta}}{\partial z} = i\boldsymbol{A}(z).\boldsymbol{\beta}\,, \tag{1.21}$$

where the 4×4 matrix $\boldsymbol{A}(z)$ has the particular elements

$$\boldsymbol{A}(z)=\begin{pmatrix} -\frac{k_x\varepsilon_{zx}}{\varepsilon_{zz}} & -\frac{k_x\varepsilon_{zy}}{\varepsilon_{zz}} & \frac{k_xk_y}{k_0\varepsilon_{zz}} & k_0\left(1-\frac{k_x^2}{k_0^2\varepsilon_{zz}}\right) \\ -\frac{k_y\varepsilon_{zx}}{\varepsilon_{zz}} & -\frac{k_y\varepsilon_{zy}}{\varepsilon_{zz}} & k_0\left(-1+\frac{k_y^2}{k_0^2\varepsilon_{zz}}\right) & -\frac{k_xk_y}{k_0\varepsilon_{zz}} \\ k_0\left(-\frac{k_xk_y}{k_0^2}-\varepsilon_{yx}+\frac{\varepsilon_{yz}\varepsilon_{zx}}{\varepsilon_{zz}}\right) & k_0\left(-\frac{k_x^2}{k_0^2}-\varepsilon_{yy}+\frac{\varepsilon_{yz}\varepsilon_{zy}}{\varepsilon_{zz}}\right) & -\frac{k_y\varepsilon_{yz}}{\varepsilon_{zz}} & \frac{k_x\varepsilon_{yz}}{\varepsilon_{zz}} \\ k_0\left(-\frac{k_y^2}{k_0^2}+\varepsilon_{xx}-\frac{\varepsilon_{xz}\varepsilon_{zx}}{\varepsilon_{zz}}\right) & k_0\left(-\frac{k_xk_y}{k_0^2}+\varepsilon_{xy}-\frac{\varepsilon_{xz}\varepsilon_{zy}}{\varepsilon_{zz}}\right) & \frac{k_y\varepsilon_{xz}}{\varepsilon_{zz}} & -\frac{k_x\varepsilon_{xz}}{\varepsilon_{zz}} \end{pmatrix} \tag{1.22}$$

ε_{ij}, with $i,j=x,y,z$ the elements of dielectric tensor and $k_0=2\pi/\lambda_0$ the wavenumber in free space. It is worth to mention that, in writing expressions (1.20), we have defined the dimensionless electric $\boldsymbol{e}$ and magnetic $\boldsymbol{h}$ fields related to $\boldsymbol{E}$ and $\boldsymbol{H}$ fields as follows:

$$\boldsymbol{e}=Z_0^{-1/2}\boldsymbol{E}, \qquad \epsilon_0\boldsymbol{d}=Z_0^{-1/2}\boldsymbol{D}, \qquad \boldsymbol{h}=Z_0^{1/2}\boldsymbol{H}, \qquad \mu_0\boldsymbol{b}=Z_0^{1/2}\boldsymbol{B}, \tag{1.23}$$

with $Z_0=\sqrt{\mu_0/\epsilon_0}$ the free space impedance and ε_0 and μ_0 the permittivity and permeability of free space, respectively.

5.2 Boundary condition

Let us consider a cholesteric elastomer confined between two planes at $z = 0$ and $z = d$ where the optical properties continuously depend on z and the surrounding medium is air. This implies that the elements of dielectric tensor ε_{ij} depend only on the z– coordinate. An incident electromagnetic wave, having wavevector $\boldsymbol{k}_t = (k_x, k_y)$, impinges from the left side of the cholesteric elastomer. This electromagnetic wave propagates through the sample and it is transmitted and reflected outside the medium having the structure

$$\boldsymbol{\beta}(x,y,z)=\boldsymbol{\beta}(z)\exp[k_xx+k_yy], \tag{1.24}$$

because the phase matching condition implies the continuity of the tangential components of $\boldsymbol{k}$.

The general solution of the differential equation (1.21) for electromagnetic waves propagating in homogeneous media is the superposition of four plane waves, two left-going and two right-going waves. With this in mind, we state the procedure to find the amplitudes of the transmitted (at $z = d$) and reflected waves in terms of incident waves at z=0. This implies the definition of the following quantities (Altman & Sucky, 1991):

i. The propagation matrix $U(0, z)$, that is implicitly defined by the equations

$$\boldsymbol{\beta}(z)=\boldsymbol{U}(0,z).\boldsymbol{\beta}(0), \qquad \boldsymbol{U}(0,0)=\boldsymbol{1}, \tag{1.25}$$

where $\mathbf{1}$ is the identity matrix and $\boldsymbol{U}(0,z)$ satisfies the same propagation equation (1.21) found for $\boldsymbol{\beta}$:

$$\partial_z \boldsymbol{U}(0,z) = i\boldsymbol{A}(z).\boldsymbol{U}(0,z)\,; \tag{1.26}$$

the propagation matrix gives the right-side field amplitudes of the cholesteric elastomer as function of the left-side ones.

ii. For a specific value d , the transfer matrix is defined as $\boldsymbol{U}(0,z)$.

iii. The scattering matrix $\boldsymbol{S}$, that gives the output field as function of the incident one. The matrix $\boldsymbol{S}$ is defined as:

$$\boldsymbol{\alpha}_{out} = \boldsymbol{S}.\boldsymbol{\alpha}_{in} \tag{1.27}$$

where $\boldsymbol{\alpha}_{in}$ and $\boldsymbol{\alpha}_{out}$ are the amplitudes of the in-going and out-going waves.

To find out $\boldsymbol{S}$, we must express the field, in any one of the external media, as a superposition of planes waves, by setting:

$$\boldsymbol{\beta} = \boldsymbol{T}.\boldsymbol{\alpha}; \qquad \boldsymbol{U}_{\boldsymbol{\alpha}}(0,d) = \boldsymbol{T}^{-1}.\boldsymbol{U}(0,d).\boldsymbol{T}, \tag{1.28}$$

where

$$\boldsymbol{\alpha} = (a_1^+, a_2^+, a_1^-, a_2^-)^T \,. \tag{1.29}$$

The relation $\boldsymbol{\beta} = \boldsymbol{T}.\boldsymbol{\alpha}$ can be interpreted as a basis change in the four dimensional space of the *state vectors* $\boldsymbol{\beta}$. The columns of $\boldsymbol{T}$ are the $\boldsymbol{\beta}$ vectors representing the four plane waves generated by the incident waves in the two external medium (here we assume as identical). The elements of vector $\boldsymbol{\alpha}$ are the amplitudes of the four plane wave. The choice of the new basis could be different depending on the particular problem. By setting

$$\boldsymbol{U}(\boldsymbol{\alpha}) = \begin{pmatrix} \boldsymbol{U}_{ff} & \boldsymbol{U}_{bf} \\ \boldsymbol{U}_{fb} & \boldsymbol{U}_{bb} \end{pmatrix}, \tag{1.30}$$

the scattering matrix writes:

$$\boldsymbol{S} = \begin{pmatrix} \boldsymbol{U}_{ff} - \boldsymbol{U}_{bf}\boldsymbol{U}_{bb}^{-1}\boldsymbol{U}_{fb} & \boldsymbol{U}_{bf}\boldsymbol{U}_{bb}^{-1} \\ -\boldsymbol{U}_{bb}^{-1}\boldsymbol{U}_{fb} & \boldsymbol{U}_{bb}^{-1} \end{pmatrix}. \tag{1.31}$$

In equations (1.29) and (1.30) the symbols + and *f* (- and *b*) mean forward (backward) propagating waves.

We point out that the methods of transfer and scattering matrices are very useful in studying the plane wave transmission and reflection from surfaces or a multilayered medium.

Eq. (1.21) can be formally integrated over a certain distance d of the cholesteric

$$\boldsymbol{\beta}(d) = e^{i\int_0^d \boldsymbol{A}(z')dz'} \cdot \boldsymbol{\beta}(0)\,, \tag{1.32}$$

and by straight comparison of Eqs. (1.25) and (1.32), the transfer matrix $\boldsymbol{U}(0,z)$ is defined as:

$$\boldsymbol{U}(0,d) = e^{i\int_0^d \boldsymbol{A}(z')dz'}, \tag{1.33}$$

where plane waves are incident and reflected in the half-space $z<0$ and a plane waves are transmitted on the half-space $z>d$.

It can be seen immediately that the problem of finding $\boldsymbol{U}(0,z)$ is reduced to find a method to integrate expression (1.33) on the whole cholesteric elastomer. Because of the non-homogeneity of the medium proposed here, we consider it as broken up into many thin parallel layers and treating each as if it had homogeneous anisotropic optical parameters (Berreman & Scheffer, 1970). In this way, $\boldsymbol{U}(0,z)$ is obtained by multiplying iteratively the matrix for each sublayer from $z=0$ to $z=d$.

In next section, we will show that for axial propagation in a cholesteric elastomer, and by choosing appropriately a reference system, the system (1.21) and the transfer matrix U have completely analytical solutions.

Now, we proceed to give the explicit form of the four-vector $\boldsymbol{\beta}$ for the surrounding medium (free space). As said above, the general solution of the differential equation (1.21) for electromagnetic waves propagating in homogeneous media is the superposition of forward and backward propagating waves. We consider an incident wave from left-half space with wavevector, $\boldsymbol{k}=(k_x,k_y,k_z)=k_0 n_d(\sin\theta\cos\varphi,\sin\theta\sin\varphi,\cos\theta)$, where n_d is the refractive index of surrounding medium, θ is the angle made between $\boldsymbol{k}$ and $z-axis$ and φ is the angle made between $\boldsymbol{k}$ and $x-axis$ in the $xy-plane$. For an arbitrary polarization state the solutions of (1.21) can be expressed as (Lakhtakia & Reyes, 2006; Espinosa-Ortega & Reyes, 2008):

$$\boldsymbol{\beta}(z)=\begin{pmatrix} \left(a_L\frac{i\hat{\boldsymbol{u}}-\hat{\boldsymbol{v}}_+}{\sqrt{2}}-a_R\frac{i\hat{\boldsymbol{u}}+\hat{\boldsymbol{v}}_+}{\sqrt{2}}\right)e^{ik_z z}+\left(-r_L\frac{i\hat{\boldsymbol{u}}-\hat{\boldsymbol{v}}_-}{\sqrt{2}}+r_R\frac{i\hat{\boldsymbol{u}}+\hat{\boldsymbol{v}}_-}{\sqrt{2}}\right)e^{-ik_z z} \\ -in_d\left(a_L\frac{i\hat{\boldsymbol{u}}-\hat{\boldsymbol{v}}_+}{\sqrt{2}}+a_R\frac{i\hat{\boldsymbol{u}}+\hat{\boldsymbol{v}}_+}{\sqrt{2}}\right)e^{ik_z z}+in_d\left(r_L\frac{i\hat{\boldsymbol{u}}-\hat{\boldsymbol{v}}_-}{\sqrt{2}}+r_R\frac{i\hat{\boldsymbol{u}}+\hat{\boldsymbol{v}}_-}{\sqrt{2}}\right)e^{-ik_z z} \end{pmatrix}, \quad \text{for } 0\le z, \tag{1.34}$$

where a_L, a_R represent the amplitude of incident propagating waves and r_L, r_R denote the reflection amplitude of propagating waves. The subscript indexes R and L correspond to right- and left-circularly polarized wave, respectively. The unit vectors $\hat{\boldsymbol{u}}$ and $\hat{\boldsymbol{v}}$ are defined as

$$\hat{\boldsymbol{u}}=-\hat{\boldsymbol{x}}\sin\varphi+\hat{\boldsymbol{y}}\cos\varphi \quad \text{and} \quad \hat{\boldsymbol{v}}_\pm=\mp\left(\hat{\boldsymbol{x}}\cos\varphi+\hat{\boldsymbol{y}}\sin\varphi\right)\cos\theta+\hat{\boldsymbol{z}}\sin\theta, \tag{1.35}$$

with $\hat{\boldsymbol{x}}$, $\hat{\boldsymbol{y}}$, $\hat{\boldsymbol{z}}$ the unit vectors parallel to the $x-,y-,z-axis$, respectively. In the region $z\ge d$, we write the transmitted field as

$$\boldsymbol{\beta}(z)=\begin{pmatrix} \left(t_L\frac{i\hat{\boldsymbol{u}}-\hat{\boldsymbol{v}}_+}{\sqrt{2}}-t_R\frac{i\hat{\boldsymbol{u}}+\hat{\boldsymbol{v}}_+}{\sqrt{2}}\right)e^{ik_z(z-d)}, \\ -in_d\left(t_L\frac{i\hat{\boldsymbol{u}}-\hat{\boldsymbol{v}}_+}{\sqrt{2}}+t_R\frac{i\hat{\boldsymbol{u}}+\hat{\boldsymbol{v}}_+}{\sqrt{2}}\right)e^{ik_z(z-d)} \end{pmatrix}, \quad \text{for } z\ge d. \tag{1.36}$$

At the tangential components of $\boldsymbol{e}$ and $\boldsymbol{h}$ must be continuous across the planes $z=0$ and $z=d$, the boundary values $\boldsymbol{\beta}(0)$ and $\boldsymbol{\beta}(d)$ can be fixed as:

$$\boldsymbol{\beta}(0)=\frac{1}{\sqrt{2}}\boldsymbol{Q}\cdot\begin{pmatrix}a_R\\a_L\\r_R\\r_L\end{pmatrix} \quad \text{and} \quad \boldsymbol{\beta}(d)=\frac{1}{\sqrt{2}}\boldsymbol{Q}\cdot\begin{pmatrix}t_R\\t_L\\0\\0\end{pmatrix}, \tag{1.37}$$

where

$$\boldsymbol{Q}=\begin{pmatrix}\cos\theta\cos\varphi & \cos\theta\cos\varphi & \cos\theta\cos\varphi & \cos\theta\cos\varphi\\ \cos\theta\sin\varphi & \cos\theta\sin\varphi & \cos\theta\sin\varphi & \cos\theta\sin\varphi\\ in_d\cos\theta\cos\varphi & -in_d\cos\theta\cos\varphi & in_d\cos\theta\cos\varphi & -in_d\cos\theta\cos\varphi\\ in_d\cos\theta\sin\varphi & -in_d\cos\theta\sin\varphi & in_d\cos\theta\sin\varphi & -in_d\cos\theta\sin\varphi\end{pmatrix}+\begin{pmatrix}i\sin\varphi & -i\sin\varphi & -i\sin\varphi & i\sin\varphi\\ -i\cos\varphi & i\cos\varphi & i\cos\varphi & -i\cos\varphi\\ -n_d\sin\varphi & -n_d\sin\varphi & n_d\sin\varphi & n_d\sin\varphi\\ n_d\cos\varphi & n_d\cos\varphi & -n_d\cos\varphi & -n_d\cos\varphi\end{pmatrix}. \tag{1.38}$$

If we restrict our analysis to the case when the electromagnetic wave is incident parallel to $z-axis$, the angles φ and θ equal zero and expression for $\boldsymbol{Q}$ is reduced to

$$\boldsymbol{Q}_0=\begin{pmatrix}1 & 1 & 1 & 1\\ -i & i & i & -i\\ in_d & -in_d & in_d & -in_d\\ n_d & n_d & -n_d & -n_d\end{pmatrix}. \tag{1.39}$$

Using Eqs. (1.32), (1.33) and (1.37) the problem of reflection-transmission can be established as follows

$$\begin{pmatrix}t_R\\t_L\\0\\0\end{pmatrix}=\boldsymbol{M}\cdot\begin{pmatrix}a_R\\a_L\\r_R\\r_L\end{pmatrix} \tag{1.40}$$

where $\boldsymbol{M}=\boldsymbol{Q}^{-1}\cdot\boldsymbol{U}(0,d)\cdot\boldsymbol{Q}$ and $U(0,d)$ are defined in (1.33). Notice that the matrix equation (1.40) gives a set of coupled equations relating amplitudes a_L, a_R, r_L and r_R (from $z\le 0$) to transmitted amplitudes t_L, t_R (for $z\ge d$).

The scattering matrix $\boldsymbol{S}$ relates amplitudes t_L, t_R, r_L and r_R with the incident amplitudes a_L, a_R. This relation can be expressed in terms of matrix M as follows (Avendaño et al., 2005)

$$\begin{pmatrix} t_R \\ t_L \\ r_R \\ r_L \end{pmatrix} = \boldsymbol{S}\cdot\begin{pmatrix} a_R \\ a_L \end{pmatrix} \qquad \text{with} \qquad \boldsymbol{S} = \begin{pmatrix} t_{RR} & t_{RL} \\ t_{LR} & t_{LL} \\ r_{RR} & r_{RL} \\ r_{LR} & r_{LL} \end{pmatrix}, \tag{1.41}$$

Co-polarized coefficients have both subscripts identical, and cross-polarized have different subscripts. The square of the amplitudes of t and r is the corresponding transmittance and reflectance; thus, $T_{RR} = |t_{RR}|^2$ is the transmittance corresponding to the transmission coefficient t_{RR} , and so on. In the absence of dissipation of energy inside the sample, the principle of conservation of energy must be satisfied, this means that

$$T_{RR} + T_{LR} + R_{RR} + R_{LR} = 1 \qquad \text{and} \qquad T_{RL} + T_{LL} + R_{RL} + R_{LL} = 1 . \tag{1.42}$$

Before ending this section, we mention that an alternative to find the transmission and reflection coefficients is using the expressions given by (1.30) and (1.31). Also, the system of equations (1.40) can be solved numerically to find the scattering matrix.

5.3 The Oseen transformation

Using a numerical procedure the set of coupled differential equations (1.21) can be solved in a straight way. Nevertheless, the intrinsic helical symmetry of a cholesteric elastomer allows to suggest the possibility of finding a reference system, for normally incident wave, for which the solution can be obtained analytically. For this aim, it is convenient to write the coupled equations in a frame of reference in which the matrix A is diagonal and not dependent on z propagation coordinate. This can be realized by rotating solidly and uniformly the four-vector $\boldsymbol{\beta}$ around $z-$axis, with the principal axes of ε_{ij} making constant angles with z . The required transformation can be realized by setting:

$$\tilde{\boldsymbol{\beta}} = \begin{pmatrix} \tilde{e}_x \\ \tilde{e}_y \\ \tilde{h}_x \\ \tilde{h}_y \end{pmatrix} = \boldsymbol{\mathcal{R}}(-qz).\boldsymbol{\beta} \qquad \text{and} \qquad \boldsymbol{H} = \boldsymbol{\mathcal{R}}(-qz).\boldsymbol{A}(z).\boldsymbol{\mathcal{R}}(qz) \tag{1.43}$$

with $\boldsymbol{\mathcal{R}}(qz)$ the rotation matrix defined as

$$\boldsymbol{\mathcal{R}}(qz) = \exp(\mathbf{R}qz) \equiv \cos qz\mathbf{1} + \sin qz\mathbf{R}, \qquad \mathbf{R} = \begin{pmatrix} 0 & -1 & 0 & 0 \\ 1 & 0 & 0 & 0 \\ 0 & 0 & 0 & -1 \\ 0 & 0 & 1 & 0 \end{pmatrix}, \tag{1.44}$$

$q = q_o / \eta$ and 1I the 4×4 identity matrix. This transformation is known as Oseen's transformation (Oseen, 1933). For axial propagation and by considering the explicit form of dielectric tensor ε_{ij} for the cholesteric elastomer, the Eqs. (1.21) are reduced to

$$\frac{d\tilde{\boldsymbol{\beta}}}{dz'} = i\boldsymbol{H}.\tilde{\boldsymbol{\beta}} , \tag{1.45}$$

the matrix $\boldsymbol{H}$ is given by

$$\boldsymbol{H}=\begin{pmatrix} 0 & -iq & 0 & 2\pi\lambda^{-1} \\ iq & 0 & -2\pi\lambda^{-1} & 0 \\ 0 & -2\pi\epsilon_{\perp}\lambda^{-1} & 0 & -iq \\ 2\pi\epsilon_{\parallel}\lambda^{-1}\epsilon(\eta) & 0 & iq & 0 \end{pmatrix} \tag{1.46}$$

and

$$\epsilon(\eta)=\frac{\epsilon_{\perp}}{\epsilon_{\perp}\sin^2\alpha(\eta)+\epsilon_{\parallel}\cos^2\alpha(\eta)} \tag{1.47}$$

λ is the wavelength in free space. Here $\epsilon_{\parallel}$ and $\epsilon_{\perp}$ represent the principal values of ϵ and μ in the rotating frame with axes x_1, x_2, z. In what follows, and to simplify notation, we omit the symbol $(\sim)$ of four-vector $\tilde{\boldsymbol{\beta}}$, $\tilde{\mathbf{e}}$ and $\tilde{\mathbf{h}}$. Unless we say the contrary, by writing $\boldsymbol{\beta}$, $\boldsymbol{e}$ and $\boldsymbol{h}$, we will always mean the fields in the rotating frame and z the dimensionless variable.
Since the system matrix $\boldsymbol{H}$ is $z-$independent, the propagation equation (1.45) admits four solutions having the form of plane waves

$$\boldsymbol{\beta}^j(z)=\boldsymbol{t}^j\exp(in_j z), \tag{1.48}$$

where $n_j, \boldsymbol{t}^j$ are the eigenvalues and eigenvectors of $\boldsymbol{H}$, respectively. They are given by:

$$\begin{aligned} n_{1,2}^2 &= \frac{4\pi^2\epsilon_m \mp 2\pi u}{\lambda^2}+q^2, \\ \boldsymbol{t}_1^{\pm} &= c_1\left(\pm n_1u_1\lambda, i\lambda q(4\pi\epsilon_m+u_1), \mp 2iq\epsilon_m n_1\lambda^2, 2\epsilon_{\parallel}\epsilon(\eta)\pi u_1+2\epsilon_m q^2\lambda^2\right), \\ \boldsymbol{t}_2^{\pm} &= c_2\left(\pm n_2u_2\lambda, i\lambda q(4\pi\epsilon_m+u_2), \mp 2iq\epsilon_m n_2\lambda^2, 2\epsilon_{\parallel}\epsilon(\eta)\pi u_2+2\epsilon_m q^2\lambda^2\right), \end{aligned} \tag{1.49}$$

where

$$\begin{aligned} u &= 2\sqrt{a_c^2\pi^2+\epsilon_m q^2\lambda^2}, \qquad u_{1,2}=2a_c\pi\mp u, \\ c_k &= \left|4n_k\lambda\left(\pi\epsilon_{\parallel}\epsilon(\eta)u_k^2+2\epsilon_m q^2\lambda^2(2\pi\epsilon_m+u_k)\right)\right|^{-1/2}, \quad (k=1,2) \\ a_c &= \frac{\epsilon_{\parallel}\epsilon(\eta)-\epsilon_{\perp}}{2}, \qquad \epsilon_m=\frac{\epsilon_{\parallel}\epsilon(\eta)+\epsilon_{\perp}}{2}. \end{aligned} \tag{1.50}$$

As shows (1.48) the internal field can be represented as a superposition of the four eigenwaves (*amplitude representation*), by setting

$$\boldsymbol{\beta}(z)=a_j\boldsymbol{t}^j\exp(in_j z)\equiv \boldsymbol{T}.\boldsymbol{\alpha}(z), \tag{1.51}$$

where $\boldsymbol{T}$ is the matrix whose $j-th$ column coincides with t^j and $\boldsymbol{\alpha}(z)$ is the 4-vector with components $a_j\exp(in_j z)$. Obviously, $\boldsymbol{\alpha}$ and $\boldsymbol{\beta}=\boldsymbol{T}.\boldsymbol{\alpha}$ represent the same state in two different sets of basis vectors. The metrization of the state space is obtained by defining a metric

tensor $\boldsymbol{G}$ and a scalar product $\boldsymbol{\beta}_1^{\dagger}.\boldsymbol{G}_{\beta}.\boldsymbol{\beta}_2 \equiv \boldsymbol{\alpha}_1^{\dagger}.\boldsymbol{G}_{\boldsymbol{\alpha}}.\boldsymbol{\alpha}_2$, where $\boldsymbol{G}_{\boldsymbol{\beta}}$ and $\boldsymbol{G}_{\boldsymbol{\alpha}} = \boldsymbol{T}^{\dagger}.\boldsymbol{G}_{\beta}.\boldsymbol{T}$ are the matrices representing $\boldsymbol{G}$ in the two sets of basis vectors. Setting

$$\boldsymbol{G}_{\beta} = \begin{pmatrix} 0 & 0 & 0 & 1 \\ 0 & 0 & -1 & 0 \\ 0 & -1 & 0 & 0 \\ 1 & 0 & 0 & 0 \end{pmatrix}, \tag{1.52}$$

the norm of the state vector represents the time average of the $z-$component of the Poynting vector, and the tensor $\boldsymbol{G}$ satisfies the relation $\boldsymbol{G} \equiv \boldsymbol{G}^{\dagger} \equiv \boldsymbol{G}^{-1}$.

In lossless media the $z-$ derivative of the norm is identically zero and the matrix $\boldsymbol{G}_{\boldsymbol{\beta}}.\boldsymbol{H}$ is self-adjoint: $\boldsymbol{G}_{\boldsymbol{\beta}}.\boldsymbol{H} = (\boldsymbol{G}_{\boldsymbol{\beta}}.\boldsymbol{H})^{\dagger} \equiv \boldsymbol{H}^{\dagger}.\boldsymbol{G}_{\beta}$. This property and the fact that the eigenvalue equation for H is biquadratic imply that the eigenvalues are $n_1, n_2, n_3 = -n_1, n_4 = -n_2$, with n_j real or purely imaginary. It is worth mentioning that the normalization constants c_1, c_2 were obtained using the metric tensor $\boldsymbol{G}$; this means that $c_k = \left| t_k^{*} G t_k \right|^{-1/2}$ with $k = 1,2$, and t_k^{*} is the conjugated complex of eigenvectors t_k.

Only the modes n_1 show a band gap for λ within the interval defined for the positive roots of equation $n_1 = 0$. Band edges are given by $\lambda_1 = 2\pi\eta\sqrt{\epsilon_{\perp}}\,/\,q_o$ and $\lambda_2 = 2\pi\eta\sqrt{\epsilon_{\parallel}\epsilon(\eta)}\,/\,q_o$. Here, the modes n_1 are pure imaginary and their corresponding eigenvectors $1^{\pm}$ define evanescent and linearly polarized standing waves. The central wavelength of the bandgap is

$$\lambda_c = \frac{\lambda_1 + \lambda_2}{2} = \frac{p\eta\sqrt{\epsilon_{\perp}}}{2}\left(1 + \sqrt{\frac{\epsilon_{\parallel}}{\epsilon_{\perp} + \epsilon_a\left(\eta^{3/2} - 1\right)/(r-1)}} \right) \tag{1.53}$$

where Eqs. (1.19) and (1.47) were substituted in the last equation. This equation demonstrates clearly that for a positively anisotropic elastomer, the reflected wavelength λ_c increases by stretching the sample along the helix axis. This behaviour is in qualitative agreement with the biaxial extension experiments performed by Finkelmann et al. (Finkelmann et al., 2001) in which λ_c decreases due to an effective compression along the helix axis. We finally observe that within the gap the polarization of the propagating eigenwaves $2^{\pm}$ is nearly circular and, in general, they are elliptically polarized.

6. Reflection bands of distorted elastomers with and without defects

It is a known fact that structural chiral materials presents the circular Bragg phenomenon in a wavelength regime (Hirota et al., 2008), where normal incident electromagnetic plane waves of left- and right-circular polarization states are reflected and transmitted differently, i. e., light of right handedness is highly reflected in a right helical structure whereas a similar plane wave but of the reverse handedness is not. Thus, structural chiral materials are circular-polarization rejection filters in optics (Avendaño et al., 2005; de Gennes & Prost, 1993; Macleod, 2001). In addition, cholesteric elastomers are very sensitive to external stimuli as electric fields, temperature and mechanical stress. Therefore, it is possible to control the Bragg regime with these sorts of stimuli. Cholesteric elastomers are formed by monomers of liquid crystals cross-linked to polymeric chains that produces a flexible

material whose molecular order is similar to cholesteric liquid crystals with the advantage that in this new material it is feasible to change the optical properties by means of macroscopic deformations. In this section we focus in the control of circular Bragg phenomenon under the influence of an externally induced mechanical strain applied parallel to the helical axis of a slab of cholesteric elastomer.

One or more defects in a periodic structure may give rise to resonant modes inside the photonic band gaps, namely standing waves with huge energy density localized in the proximity of the defects (defect modes). A conventional 1D structure with only one defect can be considered as a Fabry-Perot interferometer in which the reflecting layers at the two sides of the cavity are constituted by 1D crystals whose thickness is comparable with the attenuation length of the standing waves within the gap, which are exponentially attenuated. The cavity acts here as a defect in the periodic structure. Very interesting optical properties are obtained by considering: 1) anisotropic periodic structures, which display two different sets of band gaps for light with different polarization states, and 2) samples with more than one defect.

In this section we also consider theoretically light propagation along the helix axis of samples in which the periodic structures are cholesteric elastomers and the thickness of the cavities goes to zero. Any defect reduces therefore to a simple discontinuity plane within the periodic structure. Such samples can be obtained as follows: 1) we consider first an cholesteric elastomer without defects between planes orthogonal to the helix axis; 2) then we cut the sample in such a way to obtain two or more layers between parallel planes; and 3) we finally rotate any layer with respect to the preceding one around their common helix axis by a given angle ξ (twist angle) (Lakhtakia, 2000; Schmidtke et al., 2003; Ozaki et al., 2003; Song et al., 2004).

Some interesting numerical results have already been found recently for helical photonic crystals with only one twist defect (Becchi et al., 2004; Hodgkinson et al., 2000; Kopp & Genack, 2002; Schimdtke & Stille, 2003; Wang & Lakhtakia, 2003; Oldano, 2003; Kopp & Genack, 2003). Here we present a theoretical and analytical approach for samples with any number of twist defects under the action of axial strain.

6.1 Mechanical control of optical spectra in a cholesteric elastomer without defects

The reflectances and transmittances obtained from the scattering matrix or the transfer matrix are in terms of the elongation η, the wavelength λ and the incidence angles of light, θ (angle between the light direction and the helical axis) and φ (angle between the light direction and the $x-$axis). By numerically solving the set of equations (1.40) for oblique incidence we obtained these optical spectra for a sample of siloxane backbone chain reacting with 90% mol and 10% of the flexible difunctional cross-linking groups (di-11UB). The rod like mesogenic groups are present in the proportion 4:1 between the nematic 4-pentylphenyl-4'-(4-buteneoxy) benzoate (PBB) and the derivative of chiral cholesterol penteonate (ChP) (Cicuta et al., 2002). The behaviour of the optical spectra for another material is expected to be qualitatively similar to the presented here; the material parameters are: $r = 1.16,\ L = 10.7\mu m,\ \mathrm{p}/2 = 214nm,\ \epsilon_{\perp} = 1.91,\ \epsilon_{\shortparallel} = 2.22, \mu = 1$.

The optical spectra show a circular Bragg regime in the R_{RR} co-polarized transmittances and reflectances, which depends on the axial elongation of the cholesteric and the incidence angles of light. These spectra are consistent with the circular Bragg phenomenon for which the right

circularly polarized wave impinging a right-handed elastomer, is highly reflected, while the left circularly polarized wave is transmitted, as we can see in Fig. 3, for reflectances
We see in this figure that the center of the bandgap blue-shifts as the incidence angle increases, as it occurs in the absence of stress. We also observe that by increasing the elongation, the band width decreases as can be seen by comparing the right and the left hand columns of this figure, that correspond to $\eta = 1$ (elastomer under no deformation) and $\eta_m = 1 + (\eta_M - 1) / 2 = 1.052$ (elastomer submitted to half of its critical elongation). Moreover, when the strain is the critical $\eta_M = 1.162^{2/3} = 1.1040$, the bandgap disappears due to the fact the cholesteric director is completely aligned with the helical axis as can be observed in Fig. 4. This effect opens up the door for proposing novel devices to mechanically control the light flow, since it allows to switch off a bandgap by applying a mechanical stress to the elastomer. This is clearly illustrated in Fig. 4 where the bandwidth diminishes as a function of the deformation for normal incidence. Further results confirm the displacement of the band reflection for R_{RR} for larger incidence angles as η get larger (Espinosa-Ortega & Reyes, 2008). Therefore, these results show the possibility of mechanically control the circular Bragg phenomenon for tuning and switching applications. On the other hand, analytical results show that the reflected wavelength at normal incidence red-shifts by stretching the elastomer along the helical axis.

6.2 Optical spectra of elastomers with defects under axial strain

In the last section the mechanical control of optical spectra in a slab of cholesteric elastomer was studied. The light impinges on the slab at normal and oblique incidence. The solutions are found performing a numerical integration to find the transmission and reflection coefficients as a function of the mechanical elongation and the incidence angles. However the strongest results are in normal incidence where an analytical solution of the problem is found. Particularly, if a twist defect with $\xi = \pi / 2$ is introduced in the center of the slab, it causes a break of the symmetry that gives rise to a peak in transmission, in the middle of the Bragg regime. Thus, in the case of normal incidence, the wavelength of this peak, as a function of the elongation η, is easy to find from the results for a slab without defect. As said above the band gap and transmittance of a cholesteric elastomer can be controlled by elongating the material along its helix axis, then, the elastically control of the lasing in a cholesteric elastomer is deduced.
A result that was shown in the last section is that the axial elongation in a cholesteric elastomer close the band gap when the cholesteric director is fully oriented along the helix axes. This effect is a consequence of the presence of optical axis in the locally anisotropic material forming the sample, which in turn originates the existence of a pseudoisotropic curve. In this section we explore the optical properties around this curve and its effect over the dwell time by means of the analytical results for normal incidence. The enhancement of the dwell time is desirable for optical application, hence, the conditions in which this occurs shall widely explored (Mota et al., 2010). Finally, the mechanical tuning of two or more defect modes in the cholesteric elastomer is explored by taking into account the coupling and interference among the various defect modes.

6.2.1 Singlets

We consider now a sample between the planes $z = -\ell$ and $z = +\ell$ with only one twist defect at $z = 0$, which divides the sample in two regions referred to as a for $z < 0$ and b for $z > 0$. Next, we approach the problem quantitatively by means of exact equations for normal incidence.

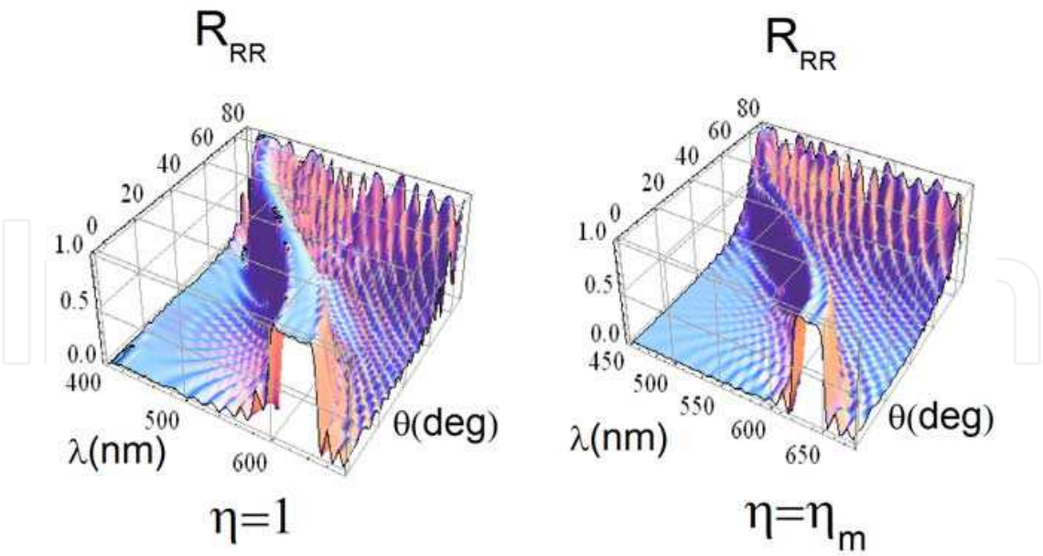

Fig. 3. Co-polarized reflectance R_{RR} versus the wavelength λ and the incidence angle θ for the elongations $\eta = 1$ and $\eta = \eta_m$.

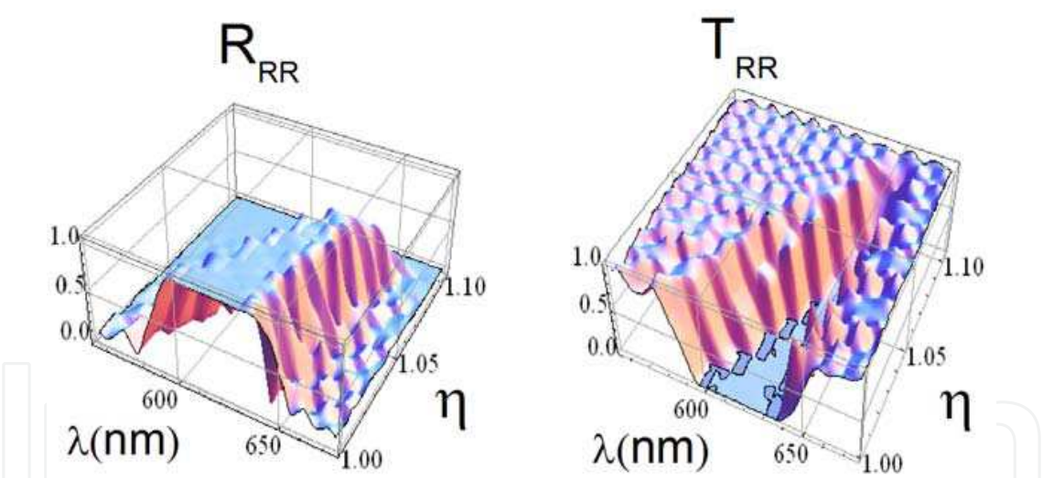

Fig. 4. Co-polarized transmittances T_{RR} and reflectances R_{RR} as a function of the wavelength λ and the axial elongation η for normal incidence.

6.2.1.1 Thick samples

Let us first consider an unbounded structure, i.e., the limit $l \to \infty$. Any solution of Maxwell equations can be written as $\boldsymbol{\beta}(z) = \boldsymbol{\beta}_a(z)\Theta(z) + \boldsymbol{\beta}_b(z)\Theta(-z)$, where $\Theta(z)$ is the Heaviside step function and $\boldsymbol{\beta}_k(z) = \mathbf{T}_k\boldsymbol{\alpha}_k(z)$ $(k = a,b)$ is a linear combination of the eigenwaves $\mathbf{t}_k^j \exp(in_j z)$ defined above in Eq. (1.48). Again, we mention that the choice of vector α_k is the same as expressed in (1.29). The eigenvectors t_a^j and t_b^j are given by Eq. (1.49) in two different frames a and b whose axes x_{2a}, x_{2b} make an angle ξ . In a frame having as axis x_2 the bisector

of x_{2a}, x_{2b}, such vectors are obtained by applying the rotation matrices $\boldsymbol{\mathcal{R}}(-\xi/2)$ and $\boldsymbol{\mathcal{R}}(\xi/2)$ to the vectors t^j defined by Eq. (1.49). The corresponding matrices $\boldsymbol{T}_a$ and $\boldsymbol{T}_b$ are therefore given by

$$\boldsymbol{T}_a = \boldsymbol{\mathcal{R}}(-\xi/2).\boldsymbol{T}, \qquad \boldsymbol{T}_b = \boldsymbol{\mathcal{R}}(\xi/2).\boldsymbol{T}. \tag{1.54}$$

In the limit $\ell \to \infty$ the exponential factors of the first component of $\boldsymbol{\alpha}_a = \boldsymbol{T}_a^{-1}.\boldsymbol{\beta}_a$ and of the third component of $\boldsymbol{\alpha}_b = \boldsymbol{T}_b^{-1}.\boldsymbol{\beta}_b$ (corresponding to the eigenwaves 1^+ in the region a and 1^- in the region b), diverge for z going to $-\infty$ and $+\infty$, respectively. Their amplitude must therefore be zero. The tangential continuity of the vectors $\boldsymbol{e}$ and $\boldsymbol{h}$ at $z=0$, give four homogeneous equations for the other six components. It is found that the amplitude of the evanescent modes is much larger than that of the propagating ones at the defect frequency ω_d and the defect mode has approximately the profile $\exp(-|z|/l_d)$ whose line width is $l_d \equiv 1/n_1(\omega_d)$ (Becchi et al., 2004).

Particularly, if the twist angle is $\pi/2$, the frequency of the peak created by this defect in the middle of the circular Bragg regime is: $\omega_d \equiv \dfrac{\omega_1+\omega_2}{2}$ whose band width is $\Delta\omega_d \equiv \omega_1 - \omega_2$.

Also, the angle $\gamma_{em}(\omega_d)$ between the electric and magnetic field of the evanescent modes at the defect frequency, may be obtained from the components of their corresponding eigenvectors given by expressions (1.49).

Thus, the defect frequency depends on the axial elongation η and the fractional shape anisotropy r as

$$\omega_d(\eta, r) = \frac{\omega_1+\omega_2}{2} = \frac{cq_0}{\eta}\left(\frac{1}{\sqrt{\epsilon_\perp}} + \frac{1}{\sqrt{\epsilon_\parallel \epsilon(\eta, r)}}\right), \tag{1.55}$$

where c is the speed of light in vacuum and $\epsilon(\eta, r)$ is given by Eq. (1.47), and the defect wavelength $\lambda_c = 2\pi c/\omega_d$ at the center of the bandgap is given by Eq. (1.53). Fig. 5 shows λ_c versus the axial elongation η and fractional shape anisotropy r. It shows that λ_c redshifts by enlarging both η and r for oblate (a) and prolate materials (b) which allows the possibility of mechanically tune the defect mode.

In Fig. 6 the inverse line width l_d^{-1}, band width $\Delta\omega_d$, angle between the electric and magnetic field of the evanescent modes at the defect frequency $\gamma_{em}(\omega_d)$ are plotted in different scales versus η and r. In this figure we observe a locus where $\eta = \eta_M$, l_d^{-1} (l_d diverges), $\Delta\omega_d$ and $\gamma_{em}(\omega_d)$ vanish. In this locus the attenuation for the defect mode is null since $l_d^{-1} = 0$, the circular Bragg regime closes $\Delta\omega_d = 0$, and the Poynting vector is null since $\gamma_{em}(\omega_d) = 0$. We shall call this curve in the $\eta - r$ space the pseudoisotropic curve.

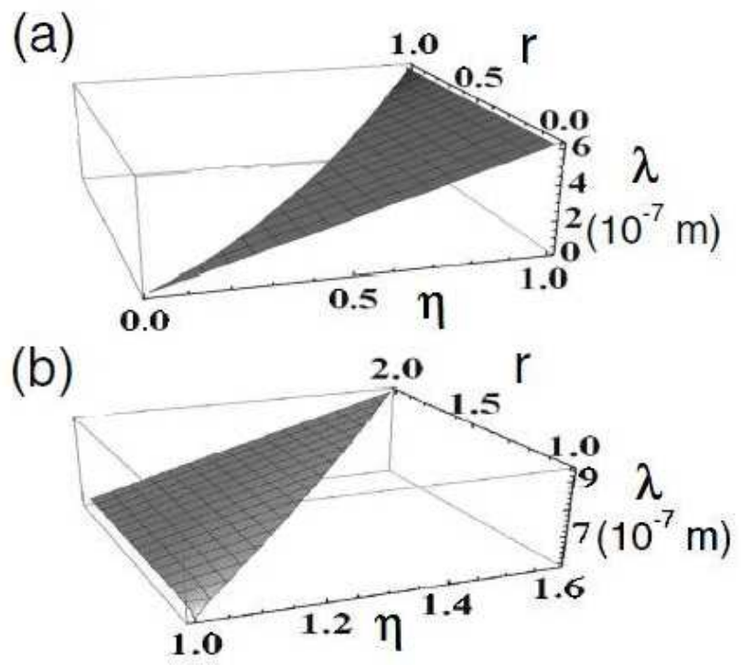

Fig. 5. Defect wavelength λ_d versus η and r for a) oblate ($0 < r < 1$) and b) ($r > 1$) prolate cholesteric elastomers axially elongated. Other parameters are, $p/2 = 214\ nm$, $\epsilon_\perp = 1.91$, $\epsilon_\parallel = 2.22$. These correspond to a typical cholesteric elastomer.

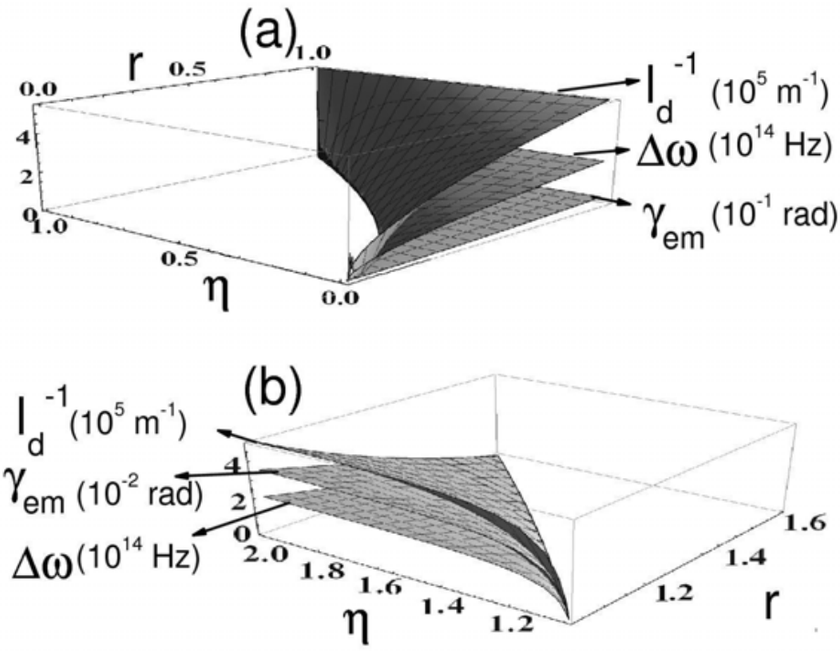

Fig. 6. Line width $l_d^{-1}(\omega_d)$, band width $\Delta\omega$ and angle between magnetic and electric field $\gamma_{em}(\omega_d)$ for the evanescent mode versus η and r. a) Oblate and b) prolate cholesteric elastomers. For the same system as Fig. 3.

This slab of cholesteric elastomer with a twist defect has potential optical applications as, for instance, Fabry-Perot resonators in lasers, hence, the enhancement of the photonic dwell time is very attractive. On the other hand, Kopp and Genack have shown that the photonic dwell time saturates versus thickness of the slab after a certain crossover thickness. It has been shown (Espinosa-Ortega & Reyes, 2008) that the deformation of the elastomer may close the band gap when the cholesteric director is fully oriented along the helix axis. This effect is a consequence of the presence of optical axis in the locally anisotropic material forming the elastomer, which in turn originates the existence of a pseudoisotropic curve (Abdulhalim, 1999). We carefully review the implications of the existence of a pseudoisotropic curve in the physical system and its effect over the photonic dwell time.

Above, it was shown that the cholesteric elastomer with a twist defect presents a pseudoisotropic curve where $\eta = \eta_M$, the line width (l_d) diverges and the band width ($\Delta\omega_d$) and angle between the electric and magnetic field ($\gamma_{em}(\omega_d)$), at the frequency defect, are null.

Therefore, for values of the axial elongation η and the fractional shape anisotropy r on the pseudoisotropic curve the following facts are found (Mota et al., 2010):

i. the transport of waves within the sample having the defect frequency is much more efficient since the attenuation for the defect mode is null, $l_d^{-1} = 0$,
ii. the circular Bragg regime closes since $\Delta\omega_d = 0$,
iii. there are no energy leaks in the sample since $\gamma_{em}(\omega_d) = 0$ amounts to a null Poynting vector.

It is worth mentioning that a pseudoisotropic curve in the $\eta - r$ space can be found when $\eta = \eta_M$ (Mota et al., 2010) with the same implications.

On the other hand, the photonic dwell time τ of this defect mode is given by the ratio between the electromagnetic energy stored by the sample and the total power of the outgoing waves. By neglecting the contribution of the propagating waves to the stored energy the dwell time dependent on the thickness of the slab, l, is found $\tau(l)$ as

$$\tau(l) \equiv \frac{l_d}{4c}\sqrt{(2\epsilon_\perp + \epsilon_\parallel)/3}\,\frac{1-\exp(-2l/l_d)}{\sin^2(\gamma_{em}/2)+\exp(-2l/l_d)} \tag{1.56}$$

whose asymptotic value for a very large sample is

$$\tau(\infty) = (l_d/(4c\sin^2(\gamma_{em}/2)))\sqrt{(2\epsilon_\perp + \epsilon_\parallel)/3}\,. \tag{1.57}$$

If, however, the CE is tuned on the pseudo-isotropic curve, $\tau(l)$ reduces to

$$\tau(l) = (l/2c)\sqrt{(2\epsilon_\perp + \epsilon_\parallel)/3}\,, \tag{1.58}$$

which now depends proportionally on the sample thickness and hence never gets bounded as it occurs for a point outside of the mentioned curve. Hence, the photon dwell time can be prolonged without limit by enlarging the sample thickness l, that opposes the behaviour reported by Kopp and Genak for cholesteric liquid crystals (Kopp & Genack, 2002).

In Fig. 7 it is depicted the inverse relative line width $\tau\omega_d$ at the defect frequency (dimensionless dwell time) which is proportional to the dwell time τ, versus the sample

thickness l and η for a) an oblate, $r = 0.5$, and b) a prolate, $r = 1.16$ cholesteric elastomer, with wave number $q_0 = \pi / (214 \times 10^{-9})\ m^{-1}$ and shows how a sharp protrusion increases its amplitude around the pseudoisotropic curve, whereas the other points in the $l - \eta$ plane remains at the smaller value of $\tau\omega_d \sim 10^7$. It is worth mentioning that the density of photonic states D at the defect frequency (Ashcroft & Mermin, 1976): $D(\omega_d) \equiv l\partial n_1(\omega_d) / \partial\omega$ can be analytically obtained from Eq. (1.49). It is easy to show that $D(\omega_d)$ diverges at the pseudo-isotropic curve. Moreover, a similar behaviour in the dwell time, around the pseudoisotropic curve, is found when it is plotted versus the axial elongation and the wave number for an oblate and a prolate cholesteric elastomer (Mota et al., 2010).
Therefore, a slab of cholesteric elastomer presents a pseudoisotropic curve where the propagation of waves in the sample with the defect frequency is extremely efficient since the attenuation for the defect mode is quite small, and the energy loses in the sample are negligible due to an almost vanishing Poynting vector. These facts support the following main results: around a pseudoisotropic curve the behaviour of the photonic dwell time has a tremendous variation and the density of photonic states diverges there.

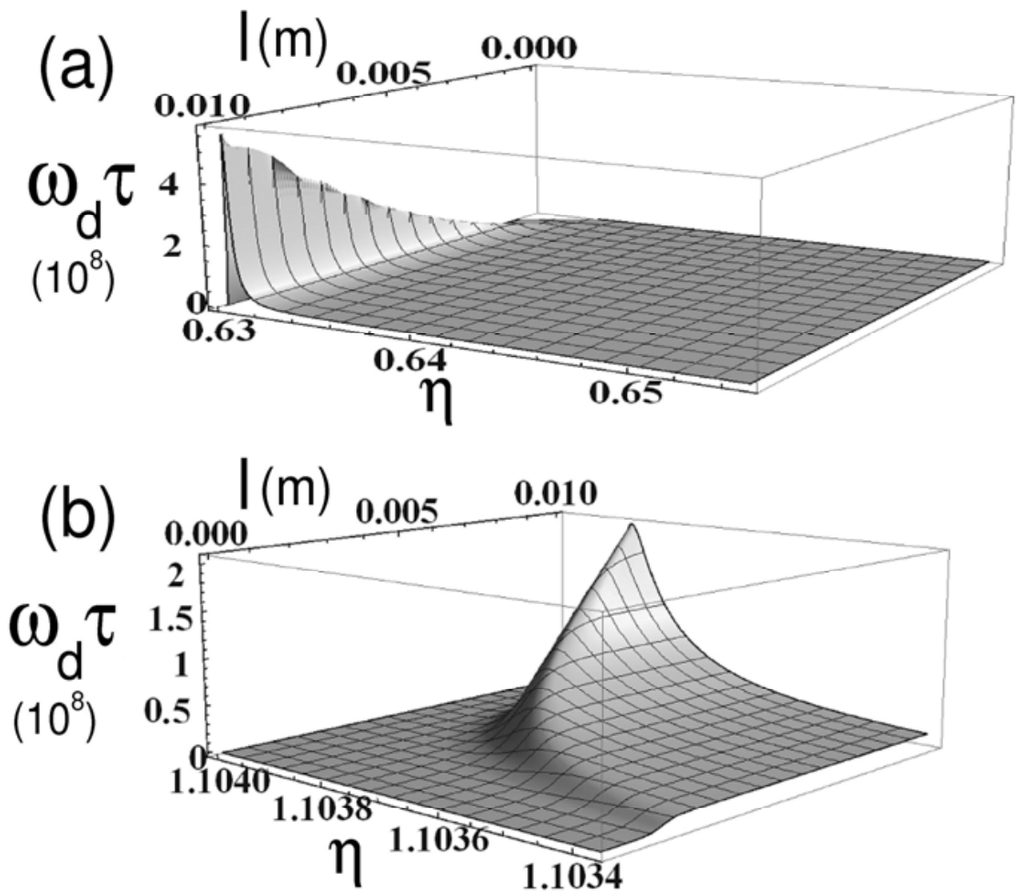

Fig. 7. $\tau\omega_d$ versus l (m) and η . For a) an oblate ($r = 0.5$) and b) a prolate ($r = 1.16$) cholesteric elastomer. For the same system as Fig. 3.

6.2.1.2 Thin samples

When the thickness $2l$ of the sample is comparable with the attenuation length l_d of the modes $1^{\pm}$, all the eigenwaves can reach the defect plane. According to the transfer matrix method seen above, we consider first the transfer matrix $\boldsymbol{U}$, which is, implicitly defined by the equation $\boldsymbol{\alpha}_b(0^+) = \boldsymbol{U}.\boldsymbol{\alpha}_a(0^-)$. Taking into account Eq. (1.54), the relation $\boldsymbol{\beta} = \boldsymbol{T}.\boldsymbol{\alpha}$, and the continuity of $\boldsymbol{\beta}(z)$ at the defect site $z = 0$, one obtains:

$$\boldsymbol{U} = \boldsymbol{U}\left(0^+, 0^-\right) = \boldsymbol{T}^{-1}.\exp(-\boldsymbol{R}\xi).\boldsymbol{T} \equiv \cos\xi\mathbf{1} - \sin\xi\boldsymbol{R}_S\,, \tag{1.59}$$

where $\boldsymbol{R}_S = \boldsymbol{T}^{-1}.\boldsymbol{R}.\boldsymbol{T}$. Straightforward calculations give

$$\boldsymbol{R}_S = \begin{pmatrix} r_1 & -r_5 & -r_3 & -r_5^* \\ -ir_5 & -ir_2 & -ir_5^* & ir_4 \\ r_3 & r_5^* & -r_1 & r_5 \\ ir_5^* & -ir_4 & -ir_5 & ir_2 \end{pmatrix}, \tag{1.60}$$

where the quantities r_j ($j = 1,...,5$) are

$$\begin{aligned} r_{1,3} &= 4q\lambda c_1^2[\mp\pi\epsilon_{\|}\epsilon(\eta)u_1(4\epsilon_m\pi + u_1) + \epsilon_m\lambda^2(n_1^2u_1 \mp q^2(4\epsilon_m\pi + u_1))], \\ r_{2,4} &= 4q\lambda c_2^2[\pm\pi\epsilon_{\|}\epsilon(\eta)u_2(4\epsilon_m\pi + u_2) + \epsilon_m\lambda^2(n_2^2u_2 \pm q^2(4\epsilon_m\pi + u_2))], \\ r_5 &= q\lambda c_1c_2\Big[4\epsilon_{\|}\epsilon(\eta)\pi(u_1u_2 + 2\epsilon_m(u_1 + u_2)) + 2\epsilon_m\lambda^2(in_1n_2(u_1 + u_2) + q^2(8\epsilon_m\pi + u_1 + u_2))\Big]. \end{aligned} \tag{1.61}$$

It is convenient to write the 4×4 matrix $\boldsymbol{U}$ in the form (1.30) and to consider also the matrix $\boldsymbol{U}^{-1} \equiv \cos\xi\mathbf{1} + \sin\xi\boldsymbol{R}_S$. The 2×2 submatrix $\boldsymbol{S}_{bb}$ is the inverse of $(\boldsymbol{U}^{-1})_{bb}$, that is given by

$$(\boldsymbol{U}^{-1})_{bb} = \begin{pmatrix} \cos\xi - ir_2\sin\xi & -r_5\sin\xi \\ ir_5\sin\xi & \cos\xi + r_1\sin\xi \end{pmatrix}. \tag{1.62}$$

As mentioned above, four eigenmodes from region a (or b) reach the defect plane. Thus, the scattering matrix S_{bb} it relates the amplitudes of backward waves in region a (the transmitted ones) to the backward waves from region b (the incident ones).

It is found numerically that, for $\lambda = \lambda_d$ the eigenwave 2^- impinging from region b is totally reflected at the defect plane. This means that the element (2,2) of S_{bb} is equal to zero. Therefore, the quantity λ_d is implicitly defined by the equation

$$\xi = \cot^{-1}\left[-r_1(\lambda_d)\right], \tag{1.63}$$

which is completely equivalent to expression (1.55) for the particular case $\xi = \pi/2$.

On the other hand, it is found that, for $\lambda = \lambda_d$ the eigenwave 1^- in region b generates at the other side of the layer an eigenwave 1^- with a huge amplitude.

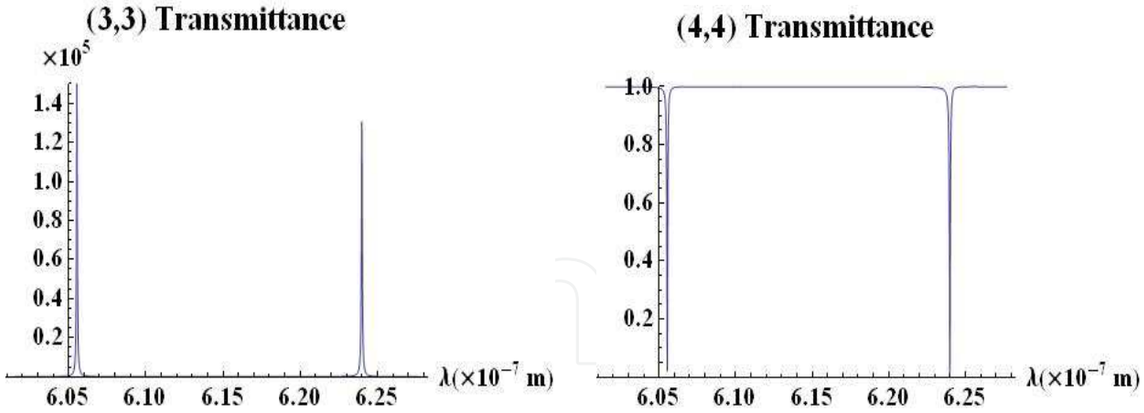

Fig. 8. Square amplitudes of the elements (3,3) and (4,4) of the scattering matrix $\boldsymbol{S}$. Here, $\theta = \pi / 2$, $\epsilon_{\|} = 2.22$, $\epsilon_{\perp} = 1.91$, $p = 428nm$, $\eta = 1$ and $r = 1.16$.

6.2.2 Doublets

Now, we consider an unbounded sample with two identical twist defects at $z = 0$ and $z = z_1$. The transfer matrix relating the $\boldsymbol{\alpha}-$ vectors at $z = 0^-$ and $z = z_1^+$ is given by

$$\boldsymbol{U} = \boldsymbol{U}\left(z_1^+, 0^-\right) = \boldsymbol{U}_1\left(\exp\left(i\boldsymbol{N}z_1\right)\right)\boldsymbol{U}_1, \tag{1.64}$$

where $\boldsymbol{U}_1$ is the transfer matrix for each one of the defect planes, given by (1.59), and $\boldsymbol{N}$ is the diagonal matrix with diagonal elements equal to n_j . The matrix $\exp\left(i\boldsymbol{N}z_1\right)$ is the transfer matrix $\boldsymbol{U}\left(z_1^-, 0^+\right)$ of the layer between the two twist defects.

The analysis presented in previous section is also valid for obtaining the transmittances and reflectances. The curves giving these quantities are quite similar to the corresponding for a single twist defect, except for the fact that they have the structure of a doublet with two defect frequencies $\lambda_{d1}, \lambda_{d2}$. The curves (3,3) and (4,4) giving the transmittance for the eigenmodes 1 and 2 are plotted in Fig. 8.

As show the plot 8 there exist two defect frequencies $\lambda_{d1}, \lambda_{d2}$ for which the eigenwave 2^- impinging from right side is totally reflected at the defect planes. This means that the element (2,2) of S_{bb} is equal to zero. Therefore, the quantity λ_d is implicitly defined by

$$\xi = \cot^{-1}\left[\sqrt{r_3^2 e^{-2z_1/l_d} - ir_5^2 e^{-z_1(in_2+1/l_d)} + ir_5^{*2} e^{-z_1(-in_2+1/l_d)}} - r_1\right]. \tag{1.65}$$

Notice that the square root terms act here as perturbing terms whose asymptotic values vanish for $z_1 \gg l_d$ and expression (1.65) becomes identical to (1.63). When $z_1 \gg l_d$ the components peaked at $z = 0$ and $z = z_1$ do not have "interaction" between them and they act independently. Thus, the defect modes become degenerated, since $\lambda_d = \lambda_{d2} = \lambda_{d1}$. By solving the Eq. (1.65) we can obtain a 3D plot of the difference $\Delta\lambda_d = \lambda_{d2} - \lambda_{d1}$ as function of shear strain η and fractional shape anisotropy r for three values of defect separation z_1 . In Fig. 9 it can be seen that the difference $\Delta\lambda_d$ of the defect frequencies vanish along the pseudoisotropic curve for any value of l_d and goes to zero as z_1 gets much bigger than l_d ; under this conditions $\lambda_d = \lambda_{d2} = \lambda_{d1}$. On the other side, notice how, at a fixed value r ,

$\Delta\lambda_d$ reaches its maximum value at $\eta = 1$ and its minimum one at the pseudoisotropic locus; this fact suggests the possibility of mechanically tune the two defect modes and the interaction between them by controlling η .

Before ending this section we mention that for both, oblate and prolate cholesteric elastomers, the defect frequencies redshift as η and r augment (curves are not shown).

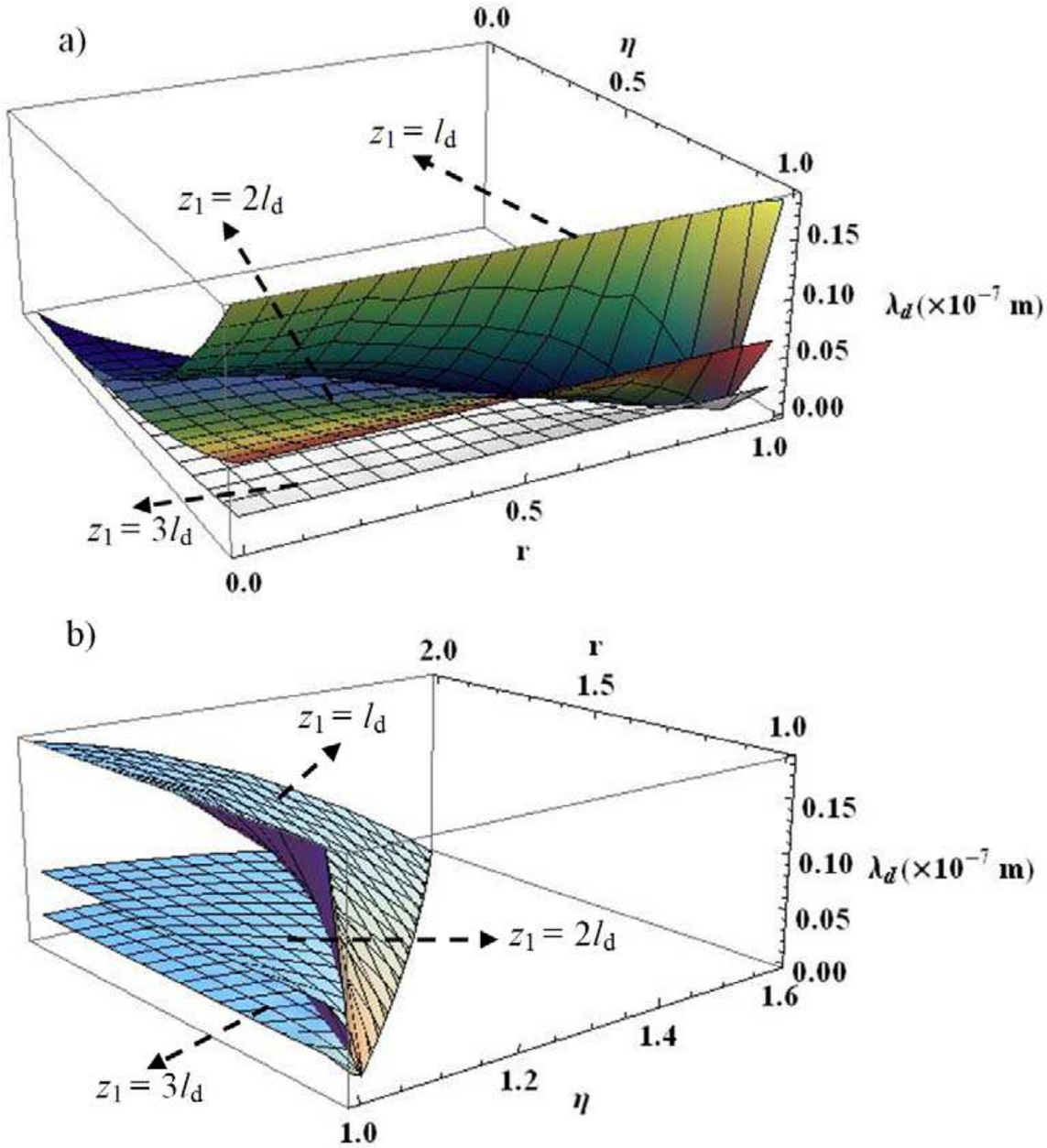

Fig. 9. Plot of the difference $\Delta\lambda_d = \lambda_{d2} - \lambda_{d1}$ as function of shear strain η and fractional shape anisotropy r for a) oblate and b) prolate cholesteric elastomers. The parameter values are the same as Fig. 8.

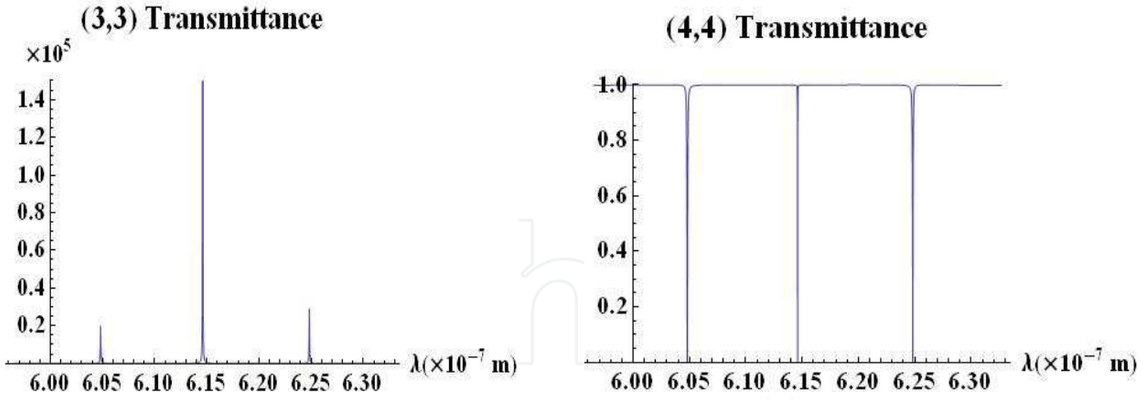

Fig. 10. Square amplitudes of the elements (3,3) and (4,4) of the scattering matrix $\boldsymbol{S}$. Here, $\theta = \pi/2$, $\epsilon_{\parallel} = 2.22$, $\epsilon_{\perp} = 1.91$, $p = 428nm$, $\eta = 1$ and $r = 1.16$.

6.2.3 Multiplets

The equation giving the transfer matrix for n_0 identical and equidistant twist defects at $z = nz_1$, where $n = 0,1,2,...,n_0 - 1$, can be written as

$$\boldsymbol{U} = \boldsymbol{U}\left((n_0 - 1)z_1^+, 0^-\right) = \boldsymbol{U}_1\left[\left(\exp(i\boldsymbol{N}z_1)\right)\boldsymbol{U}_1\right]^{n_0 - 1}. \tag{1.66}$$

For $n_0 = 2$, Eq. (1.66) becomes identical to equation (1.64). The square amplitudes of the elements (3,3) and (4,4) of the scattering matrix are plotted in Fig. 10 for $N = 3$, $\xi = \pi/2$ and $z_1 = l_d$.

The figure shows three different twist defects at the wavelengths $\lambda_{d1}, \lambda_{d2}, \lambda_{d3}$, where λ_{d2} is nearly equal to the average value of $\lambda_{d1}, \lambda_{d3}$. At the defect frequencies, the structure reflects totally the eigenwave 2. Also, it is shown that, at the defect frequencies, the eigenwave 1^- in region b generates at the other side of the layer an eigenwave 1^- with a huge amplitude.

7. References

Warner, M. & Terentjev, E. M. (2003). *Liquid Crystals Elastomers*, Oxford University Press, ISBN 0198527675, Oxford

Kac, M.; Uhlenbeck, G. E.; Hibbs, A. R. & van der Pol, B. (1976). *Probability and Related Topics in Physical Sciences*, American Mathematical Society, ISBN 0-8218-0047-7, USA

Chuang, S. L. (2009). *Physics of Photonic Devices*, (2nd. Ed.), John Wiley & Sons, ISBN 978-0-470-29319-5, New Jersey USA

Hecht, E. & Zajac, A. (1986). *Optica*, Addison-Wesley Iberoamericana, ISBN 0-201-02839-5 Delaware USA

Marcuvitz, N. & Schwinger, J. (1951). On the representation of electric and magnetic field produced by currents and discontinuities in waveguides. *Journal of Applied Physics*, 22, 806-819

Altman, C. & Sucky, K. (1991). *Reciprocity, Spatial Mapping and Time Reversal in Electromagnetics*, Kluwer Academic Publishers, ISBN 0792313399, Derdrecht The Netherlands

Berreman, D. W. & Scheffer, T. J. (1970). Bragg reflection of light from single-domain cholesteric liquid-crystal films. *Physical Review Letters*, 25, 577-581

Lakhtakia, A. & Reyes, J. A. (2008). Theory of electrically controlled exhibition of circular Bragg phenomenon by and obliquely excited structurally chiral material.*OPTIK-International Journal for Light and electron Optics*, 119, 6, 269-275

Espinosa-Ortega, T. & Reyes, J. A. (2008). Mechanically controlled bandgap in cholesteric elastomers. *Optics Communications*, 281, 5830-5837

Avendaño, C. G.; Ponti, S.; Reyes, J. A. & Oldano, C. (2005). Multiplet structure of the defect modes in 1D helical photonic crystals with twist defects. *Journal of Physics A: Mathematical and General*, 38, 8821-8840

Oseen, C. W. (1933). The theory of liquid crystals. *Transactions of the Faraday Society*, 29, 883-899

Finkelmann, H.; Kim, S. T.; Muñoz, A.; Palffy Muhoray, P. & Taheri, B. (2001). *Advanced Materials*, 13, 14, 1069-1072

Hirota, Y.; Ji, Y.; Serra, F.; Tajbakhsh, A. & Terentjev, E. (2008). Effect of crosslinking on the photonic bandgap in deformable cholesteric elastomers. *Optics Express*, 16, 5320-5331

de Gennes, P. G. & Prost, J. (1993). *The Physics of Liquid Crystals*, (2nd. Ed.), Clarendon Press, ISBN 0198520247, Oxford, UK

Macleod, H. A. (2001). *Thin-Film Optical Filters*, (3rd Ed.), Institute of Physics Bristol, ISBN 9780750306881, U. K.

Lakhtakia, A. (2000). Shear axial modes in a PCTSCM. Part V: transmission spectral holes. *Sensors and Actuators A*, 80, 216-223

Schmidtke, J.; Stille W. & Finkelmann, H. (2003). Defect mode emission of a dye doped cholesteric polymer network. *Physical Review Letters*, 90, 83902-83905

Ozaki, M.; Ozaki, R.; Matsui, T. & Yoshino, K. (2003). Twist-defect-mode lasing in photopolymerized cholesteric liquid crystal. *Japanese Journal of Applied Physics,* 42, L472-L475

Song, M. H.; Shin, K. C.; Park, B.; Takanishi, Y.; Ishikawa, K.; Watanabe, J.; Nishimura, S.; Toyooka, T.; Zhu, Z. G.; Swager, T. M. & Takezoe, H. (2004). Polarization characteristics of phase retardation defect mode in polymeric cholesteric liquid crystals. *Science and technology of Advanced Materials*, 5, 437-441

Becchi, M.; Ponti, S.; Reyes, J. A. & Oldano, C. (2004). Defect Modes in helical photonic crystals: an analytic approach. *Physical Review B*, 70, 033103-033106

Hodgkinson, J. J.; Wu, Q. H.; Thorn, K. E.; Lakhtakia, A. & McCall, M. W. (2000). Spacerless circular-polarization spectral-hole filters using chiral sculptured thin films: theory and experiment. *Optics Communications*, 184, 57-66

Kopp, V. I. & Genack, A. Z. (2002). Twist defect in chiral photonic structures. *Physical Review Letters*, 89, 033901-033904

Schmidtke, J. & Stille, W. (2003). Photonic defect modes in cholesteric liquid crystal films. *The European Physical Journal E,* 12, 553-564

Wang, F. & Lakhtakia, A. (2003). Specular and nonspecular, thicknessdependent spectral holes in a slanted chiral sculptured thin film with a central twist defect. *Optics Communications*, 215, 79-92

Oldano, C. (2003). Comment on "Twist defect in chiral photonic structures". *Physical Review Letters*, 91, 259401

Kopp, V. I. & Genack, A. Z. (2003). Kopp and Genack Reply:. *Physical Review Letters*, 91, 259402

Cicuta, P.; Tajbakhsh, A. R. & Terentjev, E. M.. (2002). Evolution of photonic structure on deformation of cholesteric elastomers. *Physical Review E*, 65, 051704-051709

Mota, A. E.; Palomares, L. O. & Reyes, J. A. (2010). Mechanically controlled defect mode in cholesteric elastomers. *Applied Physics Letters*, 96, 081906-081908

Abdulhalim, I. (1999), Point of ultra-sensitivity to perturbations for axial propagation in helicoidal bianisotropic structures, *Europhysics Letters*. 48, 2, 177

Ashcroft, N. W. & Mermin, N. D. (1976). *Solid State Physics*, Harcourt-Saunders, ISBN 0-03-083993-9, Philadelphia

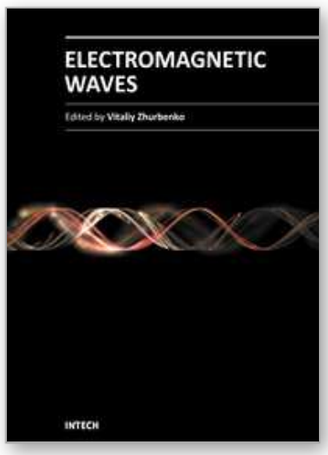

Electromagnetic Waves

Edited by Prof. Vitaliy Zhurbenko

ISBN 978-953-307-304-0
Hard cover, 510 pages
Publisher InTech
Published online 21, June, 2011
Published in print edition June, 2011

This book is dedicated to various aspects of electromagnetic wave theory and its applications in science and technology. The covered topics include the fundamental physics of electromagnetic waves, theory of electromagnetic wave propagation and scattering, methods of computational analysis, material characterization, electromagnetic properties of plasma, analysis and applications of periodic structures and waveguide components, and finally, the biological effects and medical applications of electromagnetic fields.

InTech Europe
University Campus STeP Ri
Slavka Krautzeka 83/A
51000 Rijeka, Croatia
Phone: +385 (51) 770 447
Fax: +385 (51) 686 166
www.intechopen.com

InTech China
Unit 405, Office Block, Hotel Equatorial Shanghai
No.65, Yan An Road (West), Shanghai, 200040, China
中国上海市延安西路65号上海国际贵都大饭店办公楼405单元
Phone: +86-21-62489820
Fax: +86-21-62489821

IntechOpen